Available online at www.sciencedirect.com

ScienceDirect

journal homepage: www.elsevier.com/locate/he

A first-principles study on two-dimensional tetragonal samarium nitride as a novel photocatalyst for hydrogen production

Mian Azmat [a,b], Abdul Majid [a,*], Mohammad Alkhedher [c], Sajjad Haider [d], Muhammad Saeed Akhtar [e]

[a] Department of Physics, University of Gujrat, Gujrat 50700, Pakistan
[b] Beijing Key Laboratory of Construction Tailorable Advanced Functional Materials and Green Applications, School of Materials Science and Engineering, Beijing Institute of Technology, Beijing 100081, China
[c] Mechanical and Industrial Engineering Department, Abu Dhabi University, Abu Dhabi 59911, United Arab Emirates
[d] Chemical Engineering Department, College of Engineering, King Saud University, P.O.Box 800, Riyadh 11421, Saudi Arabia
[e] School of Chemical Engineering, Yeungnam University, Gyeongsan 38541, Republic of Korea

HIGHLIGHTS

- Two-dimensional tetragonal samarium nitride.
- Structural, chemical, dynamic, thermal stability.
- Suitable band offsets for electrochemical reduction of water splitting.
- Light-harvesting ability of the material from visible/ultraviolet regions.

GRAPHICAL ABSTRACT

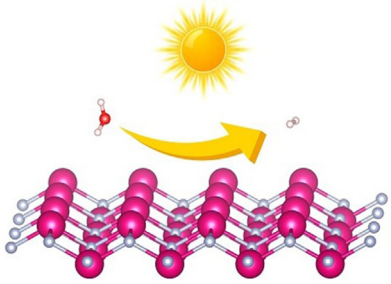

ARTICLE INFO

Article history:
Received 23 February 2023
Received in revised form
16 April 2023
Accepted 21 April 2023
Available online 7 May 2023

Keywords:
SmN
Ab-initio calculations

ABSTRACT

The prospect of using two-dimensional tetragonal samarium nitride (t-SmN) in photocatalytic applications is being reported. First principles calculations were performed in order to study structural, electronic, thermal and photocatalytic properties of the material. The phonon band structure and cohesive energy computed using density functional perturbation theory revealed dynamical stability of the monolayer. Ab-initio molecular dynamics (AIMD) simulations were carried out to check the thermal stability of the monolayer which pointed that the material is stable above 1000 K and chemically inert at room temperature. The electronic structure calculations revealed SmN as ferromagnetic semiconductor with a direct bandgap of 1.41 *eV* that predicts applications of the material in spintronics. The band alignment pointed towards suitability of band offsets for

* *Corresponding author.*
E-mail address: abdulmajid40@yahoo.com (A. Majid).
https://doi.org/10.1016/j.ijhydene.2023.04.248

Stability
Surface
Water splitting

electrochemical reduction of water splitting at neutral pH. The optical properties indicated decent light-harvesting ability of the material from visible and ultraviolet regions of solar spectrum. The micro-mechanisms of water decomposition and photocatalytic hydrogen formation on the SmN monolayer are unraveled to confirm water splitting and hydrogen generation.

Introduction

The spectrum of two-dimensional (2D) materials starting from graphene has extended to borophene, germanene, silicon carbide, black phosphorus, transition-metal dichalcogenides, monolayer gadolinium halides, etc. in the past decade [1–10]. The 2D materials offer unique physical properties such as thin layer thickness, transparency, flexibility, and conductivity when compared with the conventional bulk counterparts [9,11–14]. Among these 2D materials, transition metals (TM)-based monolayers are promising candidates owing to their electrocatalytic and photocatalytic properties [15–17]. These exhibit rich active sites for chemical reactions due to their large surface area. The photocatalysts are capable to produce hydrogen by splitting water via visible light which points to their potential to solve impending energy crisis by harvesting the solar energy [18]. The outcomes of extensive global research activities appeared to synthesize several efficient TM-based monolayer photocatalysts such as TiO_2 [19], WS_2 [20], and ZnO [21] while predictions on RhTeCl [22], Zr_2CO_2 [23] and FeS_2 [15] have been made.

The performance of a photocatalyst can be gauged on basis of several factors. An ideal photocatalyst to efficiently split water molecules should have bandgap larger than 1.23 eV and smaller than 3.0 eV in order to harvest sunlight. The position of bottom of the electronic conduction band minimum needs to be higher than −4.44 eV i.e., reduction potential of H^+/H_2 whereas the top of the valence band should be lower than −5.67 eV i.e., oxidation potential of O_2/H_2O. The photocatalyst should have a small binding energy of photo-generated charge carrier (electron-hole pair) and low recombination rate to efficiently avoid surface charge recombination of the carriers [24,25]. These requirements are strict which appeared to hinder the practical hydrogen production upon using available 2D photocatalysts. Hence, the relevant community is striving to improve the properties of photocatalysts by adding reagents or co-catalysts. The noble metals Pd, Pt, Cr, Co, Rh, etc. are generally used as co-catalysts to improve photocatalytic activity but some of them are costly and toxic. Therefore, extensive research activities on developing potential photocatalyst fulfilling the requirements of water splitting are in progress.

Though, various TM based 2D materials have been designed and examined for photocatalytic applications but work on RE based 2D materials is scarce. The RE based 2D materials are expected to offer unique electronic properties due to 4f electrons which may be very helpful in photocatalytic activities [26]. To the best of our knowledge, 2D materials comprising of RE nitrides have not yet been reported. These considerations have motivated the authors to investigate the prospects of developing novel RE nitride monolayers. In this article, we present a first-principles study of structural, electronic, magnetic, and catalytic properties of monolayered samarium nitride. On the basis of thorough investigations, we proposed a novel 2D tetragonal-structured samarium nitride (t-SmN) which appeared a ferromagnetic semiconductor when bulk samarium nitride is sliced along the (110) plane. The dynamic, thermal, and chemical stability of monolayer SmN was established on the basis of structure optimization, phonon dispersion, and AIMD simulations. Furthermore, we studied the water dissociation adsorption on the t-SmN monolayer to explore the decomposition mechanism of water. The findings of this study revealed that monolayer SmN is a promising candidate for photo-catalyst and opto-electronics devices.

Computational method

The entire work reported herein was carried out via density functional theory (DFT) based on plane-wave basis projector-augmented wave method implemented in VASP [27]. Generalized gradient approximation (GGA) functional supported by parameterization from Perdew-Burke-Ernzerhof (PBE) was adopted to deal with exchange and correlation [28]. The standard pseudo-potential was considered for all kinds of atoms with valence electron configurations as $5s^25p^64f^55d^16s^2$ for Sm and $2s^22p^3$ for N [29,30]. The spin polarization was considered in all the calculations. The crystal structure of SmN was fully relaxed with plane-wave cut off energy set at 600 eV. The respective values of energy convergence and residual force per atom were 10^{-6} eV and 0.01 eV/Å. A vacuum space of more than 20 Å along out-of-plane direction was set to avoid any interaction between the monolayer and its periodic images. A Monkhorst-Pack k-point grids of $7 \times 7 \times 1$ and $9 \times 9 \times 1$ was used for sampling the Brillouin zone integration for structural relaxation and electronic calculations respectively.

The conventional GGA:PBE is known to underestimate the bandgap of semiconductors. A computationally more expensive Heyd-Scuseria-Ernzerhof (HSE06) hybrid functional [31] has been found suitable to reproduce the experimental values of bandgap of various systems e.g. MoS_2, TiS_3, phosphorene, and $SrZrO_3$ [32–34]. Hence, we employed HSE06 functional to obtain the electronic structures, bandgap, and optical properties from GGA:PBE relaxed geometries. The hybrid functional is also resourceful to handle the strongly correlated 4f electrons of Sm.

We performed phonon dispersion calculations using the density functional perturbation theory (DFPT) approach adopted in the PHONOPY code [5,35]. The force constant

matrix was constructed by slight atomic displacements of 4 × 4 × 1 supercell and electronic degrees of freedom were increased to 10^{-8} eV to make sure proper convergence. The ab-initio molecular dynamics (AIMD) works in a combination of different ab-initio schemes comprising of computing the electronic structure as well as molecular dynamics simulations. It helps exploration of thermal stability of many 2D materials in addition to examining the structural and electronic characters. AIMD simulations were carried out with a 4 × 4 × 1 supercell in an NVT ensemble and a Nosé-Hoover thermostat for the temperature control of systems [36]. AIMD was performed on 4 × 4 × 1 supercell of 64 atoms for 5000 steps thereby setting the time step of 2 fs which has been found sufficient to investigate the thermal stability at elevated temperatures [35].

Results and discussion

Structural properties and stability

The bulk SmN is a half-metallic ferromagnetic material having a rock salt like cubic crystal structure. In order to create a surface, SmN monolayer is prepared by slicing the bulk along (110) plane in the form of a tetragonal structure of bulk SmN whereas the square lattice is unstable. The top and side views of the 4 × 4 × 1 supercell of monolayer SmN after full structural relaxation are shown in Fig. 1. The t-SmN belongs to space group P2_1/m and its unit cell consists of two Sm and two N atoms with lattice parameters as $a = 4.6671$ Å and $b = 4.0077$ Å. The structure appeared in buckled layered form in such a way that N atom layer is sandwiched between two Sm atom layers. Each Sm(N) atom is surrounded by four N(Sm) atoms. The bond lengths of Sm(N) atoms with the four adjacent N(Sm) atoms are different. The bond length of Sm–N is 2.3806 Å and 2.2948 Å along with the a and b-directions respectively.

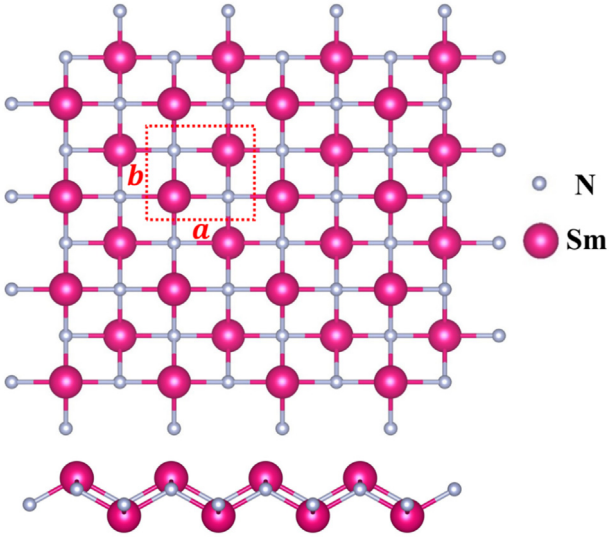

Fig. 1 – The optimized structure of 4 × 4 × 1 supercell of SmN showing the top and side views. The maroon and grey balls represent Sm and N atoms respectively.

Table 1 – A comparison of calculated cohesive energies of t-SmN monolayer and some other 2D materials.

Material	Cohesive Energy E_{coh} (eV per atom)	Experimentally obtained or not
Tetragonal SmN	7.32	No
Graphene	8.66 [39]	Yes
Silicene	3.98 [40]	Yes
ZnO	4.21 [41]	Yes
h-AlN	503 [42]	No
Tetragonal YN	5.14 [43]	No
h-GaAs	7.11 [25]	No

The stability of theoretically designed 2D materials is very crucial. Cohesive energy is a very important physical quantity to measure the kinetic stability of a material and it is defined as the energy released to crystallize the condensed material from its isolated atoms in gaseous form. The mathematical relation for cohesive energy is:

$$E_{coh} = \frac{E_{SmN}}{n_{tot}} - (n_{Sm}E_{Sm} + n_N E_N)$$

where E_{SmN} represents the total energy of SmN; E_{Sm} and E_N represent the energies of isolated single Sm and N atoms respectively; n_{tot}, n_{Sm}, and n_N stand for the total number of atoms in SmN supercell, the number of Sm and N atoms respectively. The calculated cohesive energy per atom of SmN is −7.318eV which is comparable to other 2D materials including graphene, AlN, AlP, Mo_2C, YN, TiC, and silicene [35,37,38]. The cohesive energies of the SmN monolayer and various other 2D materials are given in Table 1 which points to strong possibility to realize the SmN monolayers.

The dynamical stability of the 2D t-SmN crystal structure was also investigated by performing phonon dispersion calculations. The phonon band structure and partial DOS of the 4 × 4 × 1 supercell of SmN are shown in Fig. 2. It can be seen clearly that there is no imaginary/negative frequency in the entire Brillouin zone which points to dynamical stability of SmN monolayer. The highest phonon frequency reaches up to 18.4 THz which reflects the robust bonding between Sm and N

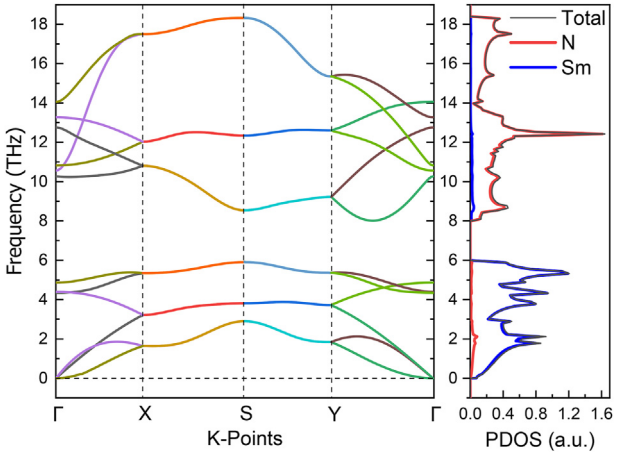

Fig. 2 – The phonon band structure calculated with 4 × 4 × 1 supercell of SmN and corresponding density of states.

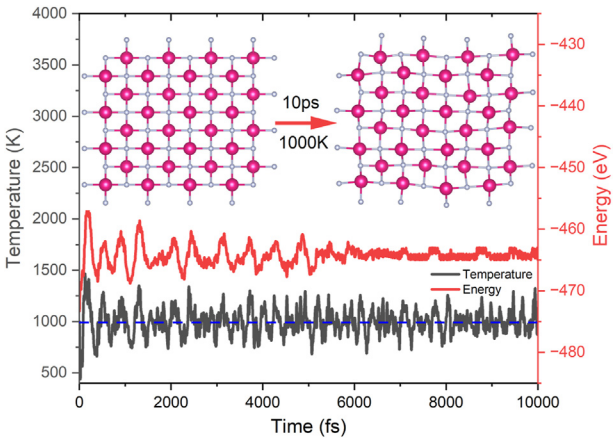

Fig. 3 – The computed results of MD simulations showing temperature and variation of free energy of the supercell of SmN monolayer as a function of time. The snapshot of the supercell at start and end of MD simulation are also shown.

atoms in the SmN monolayer. This highest phonon frequency is higher than maximum phonon frequencies of silicene (17.57 THz) [44], MoS_2 (14.33 THz) [45,46], GdX_2 (X = Cl, Br, I) [5] and AlP (16.21 THz) [35]. The phonon bandgap of 2.63 THz was observed in the acoustic and optical modes which implies that acoustic phonon modes do not interact with optical phonon modes. Recent studies have shown that the interaction of optical modes with acoustic modes causes strong scattering of acoustic phonons in heavy metal compounds and optical phonons lying in the range of acoustic modes contribute in decreasing the thermal conductivity [47–49]. The findings indicate that SmN may have a high lattice thermal conductivity.

The AIMD calculations were also performed to investigate the thermal stability of the monolayer at elevated temperatures. A 4 × 4 × 1 supercell of 64 atoms was used to perform AIMD simulation for 5000 steps with 10 ps with a time step of 2 fs at 1000 K. The energy and temperature against the time steps are plotted in Fig. 3 which also shows the snapshots taken at the start (left side) and end (right side) of the MD simulation. The total energy of the structure almost remains constant after 6 ps. The structure of 2D SmN is well maintained at 1000 K at the end of the simulation which points to thermal stability of the material at high temperature.

We further evaluated the chemical stability of SmN in the air at room temperature (300 K). A 3 × 3 × 1 supercell of 2D SmN was exposed to various gases N_2, H_2, O_2, and H_2O at very high pressure and room temperature. The density of gas molecules of 9.60 × 10^{26} molecules/m^3 was used in our MD simulations. The SmN structure did not react chemically with N_2, H_2, or O_2 molecules and remained undamaged after 1 ps which is an indicator of the chemical stability of the monolayer in air at room temperature. On the other hand, the oxygen molecules were adsorbed physically on the surface while the water reacted chemically on the SmN surface, but the crystal structure remained intact. Based on the above-discussed situations, we concluded that the 2D SmN is dynamically, thermally, and chemically stable and can be experimentally synthesized.

Electronic structures and optical properties

The structural and electronic properties of bulk SmN are performed using hybrid functional HSE06 and relaxed geometry of the structure along with the electronic band structure are shown in Fig. 4. The calculated value of lattice constant of 5.1434 Å and electronic band structure are in good agreement with experimental data [30,50,51] which points to the validity of our results on 2D t-SmN. Therefore, in order to compute the electronic properties of the SmN monolayer, we employed hybrid functional HSE06 level of theory to compute the correct energy of Sm 4f-orbitals and the electronic structure.

The calculated density of states (DOS) for 2D SmN is shown in Fig. 5 in which Fermi level is set as 0 eV. The spin polarization can be seen due to the Sm 4f-electrons. The bands present in the valence band near valence band minimum (VBM) have a major contribution of N-2p and Sm-5d states. N-2p and Sm-5d states overlap in the valence band and hybridization between 2p states of N and 5d states of Sm can be seen

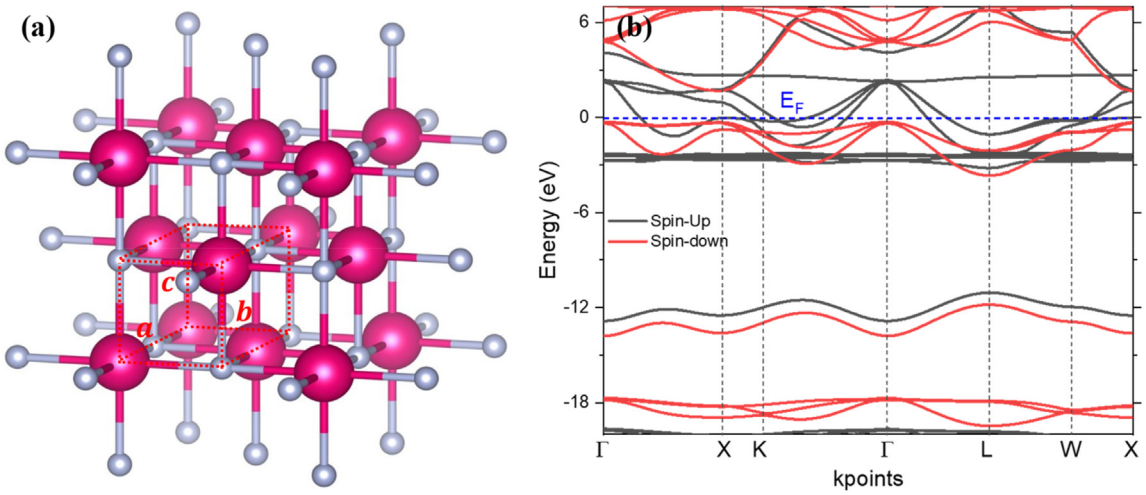

Fig. 4 – The computed results on bulk-SmN using HSE06 functional (a) crystal structure and (b) electronic band structure.

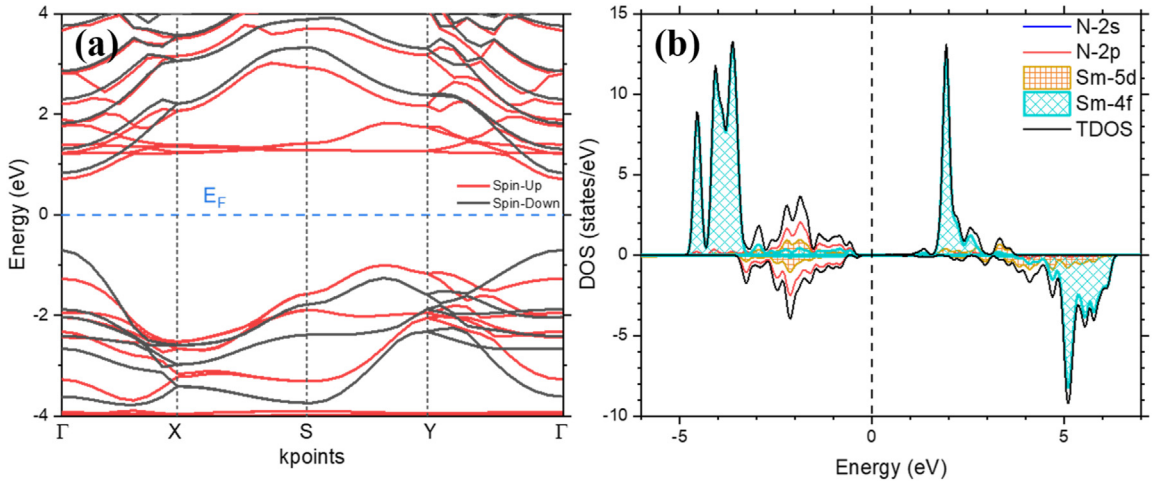

Fig. 5 – Calculated band structure (a) and density of states (b) for t-SmN monolayer by using hybrid functional HSE06.

in the valence band. The contribution of N-2p states is very small in the conduction band. The lower portion of the valence band is made up of Sm-4f spin-up localized states and is responsible for the magnetic properties of the SmN monolayer. On the other hand, the conduction band has a major contribution from Sm-4f states and a minor contribution from Sm-5d and N-2p states. The lower and upper parts of the conduction band (CB) comprised of Sm-4f spin-up and spin-down states respectively. A direct band gap of almost 1.41 eV is observed between VBM and CBM at Γ kpoint as shown in Fig. 5 (a) which indicates the semiconducting nature of SmN monolayer that points to application of the material in spintronics devices [52,53]. Further probe of electronic, optical, and magnetic properties of 2D SmN material is very necessary to completely understand this semiconductor material for its applications in future devices.

We have also studied the optical absorption of the SmN monolayer to observe its light-harvesting performance. The light absorption spectrum of the monolayer was calculated by polarized light and shown in Fig. 6. We can conclude from the absorption spectra that the monolayer is an optically anisotropic material and covers light absorption from the visible to ultraviolet region of the electromagnetic spectrum along with both *x* and *y* directions.

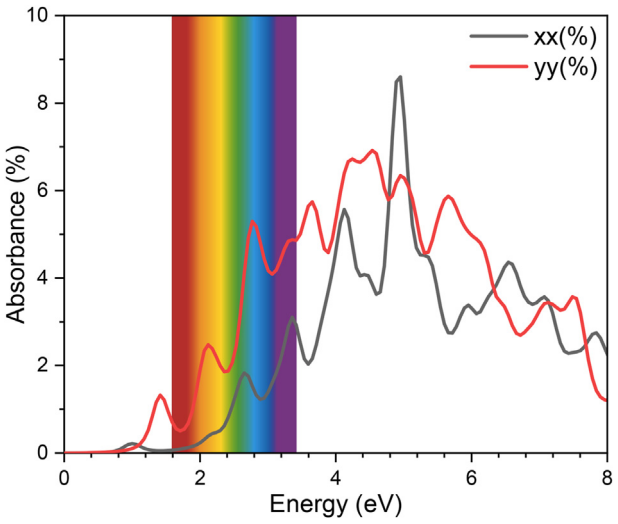

Fig. 6 – The theoretical optical absorbance spectrum of SmN monolayer computed for x- and y-directions at HSE06 level of theory.

Water splitting on t-SmN monolayer

The materials whose band gap is less than 3.0 eV and absorbs energy in the wavelength range of 400–700 nm (visible spectrum) are considered good candidates for photocatalytic reactions. The bandgap and optical absorption range of SmN lies in the visible region of light as discussed above in the electronic and optical properties, and it may show reasonable photocatalytic activity in water splitting by harvesting solar light. However, it was vital to check the stability of SmN in liquid water to investigate the actual environment of catalyst in practical applications. We employed AIMD simulations to probe the stability of the SmN monolayer in liquid water. The monolayer remains intact after 2 ps with small atomic vibration about their mean positions as shown in Fig. 7. The 50% nitrogen sites were also occupied by the hydrogen atoms as a

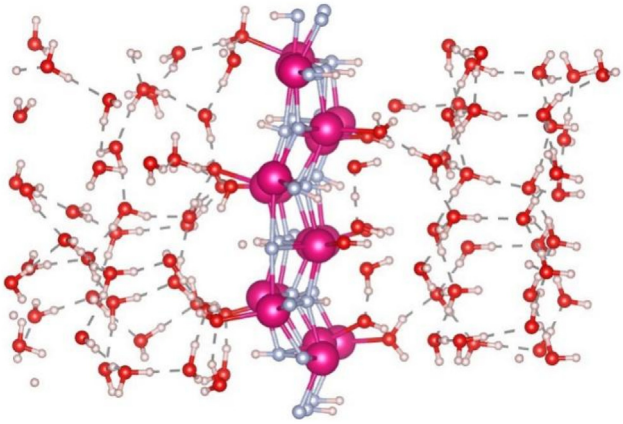

Fig. 7 – Snapshot of 3 × 3 × 1 supercell of the t-SmN monolayer in liquid water after stabilizing at 300 K after 2 ps.

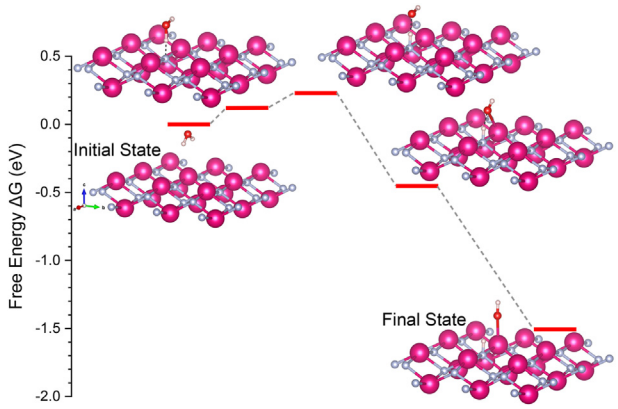

Fig. 8 – The reaction pathway of water dissociation reaction on SmN monolayer. The maroon, grey, red, and light pink balls represent Sm, N, O, and H atoms respectively. (For interpretation of the references to color in this figure legend, the reader is referred to the Web version of this article.)

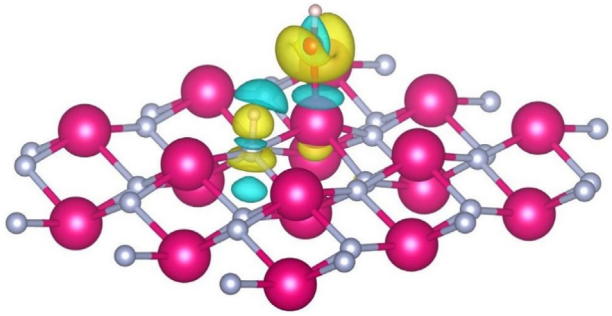

Fig. 9 – Charge density difference of dissociative adsorption of a water molecule on SmN monolayer, the yellow isosurface represents the charge accumulation and the blue one indicates the charge consumption. (For interpretation of the references to color in this figure legend, the reader is referred to the Web version of this article.)

result of water decomposition on SmN. The hydrogen atoms remain attached to nitrogen atoms, but migration of a few hydroxyl ions was observed on nearby Sm atoms or towards the hydrogen atom of the water molecules which shows the weak bonding of hydroxyl ions with Sm atoms in comparison to hydrogen-nitrogen bonding, in agreement with literature [54,55].

The water molecule dissociative adsorption has been observed on SmN monolayer which renders it an active surface for water decomposition. The most stable site for water molecule adsorption is the bridging N atom between two Sm atoms in the top layer. The reaction pathways of water molecule dissociation and energy profile are shown in Fig. 8. When water molecule came close to SmN monolayer, N atom attracted one of the hydrogen atoms of the water molecule by weakening the hydrogen-oxygen covalent bond while the other hydrogen atom went away from the monolayer. The oxygen atom of the water molecule tilted towards the Sm atom as shown in Fig. 8 that caused dissociation of the water molecule. The hydrogen and hydroxyl parts of the water were adsorbed on the N and Sm atoms of SmN monolayer respectively. Water molecule dissociation energy barrier of 0.21 *eV* is observed on the SmN surface which is smaller than water dissociation barrier for other recently studied surfaces [56–60]. The water decomposition reaction on the SmN monolayer is exothermic and irreversible. The reaction energy is 1.52 eV which is higher than the water dissociation reaction energy on the TiO_2 (001) surface and 2D Zr_2CO_2 [23,61]. The water dissociation reaction on 2D Zr_2CO_2 is endothermic. The charge density difference plot for dissociative water adsorption on the SmN monolayer is shown in Fig. 9 to further probe the mechanism. The yellow color isosurface represents the charge accumulation and the blue color indicates the charge consumption. It can be seen clearly from the blue color in Fig. 9 that the electron density decreased on the surface of SmN and charge was transferred from the surface to the water decomposition products. Above the surface, electron density first increased around the O atom of the OH group and the H atom attached to the nitrogen atom and then decreased. It means that hydrogen and hydroxyl ions of water molecules interact strongly with the surface of the SmN monolayer. From these results, we can conclude that a water molecule can be split on surface of SmN monolayer at neutral pH of 7 and which points to robustness of the material for photocatalytic reactions.

The band edge positions of a photocatalyst play very important role in production of hydrogen and oxygen from water and these must straddle the water redox potentials for this purpose. The CBM of photocatalyst should be higher than water's redox potential −4.44 eV and VBM of photocatalyst should be lower than water's oxidation potential −5.67 eV at 0 pH. These reduction and oxidation potentials vary with pH value as: $E_{reduction} = -4.44 + pH \times 0.0059$ eV, $E_{oxidation} = -5.67 + pH \times 0.0059$ eV. We calculated the absolute band edges positions of SmN monolayer to check its feasibility for hydrogen/oxygen production by water splitting using the equation $E^{Abs}_{CBM/VBM} = E^{HSE06}_{CBM/VBM} - E_{vac}$, where $E^{Abs}_{CBM/VBM}$, $E^{HSE06}_{CBM/VBM}$ and E_{vac} are the energies of absolute band edges, HSE06 calculated band edges and vacuum level respectively. The calculated values of E^{HSE06}_{CBM}, E^{HSE06}_{VBM} and V_{vac} are −2.254 *eV*, −3.667 *eV* and 0.912 *eV* respectively, hence $E^{Abs}_{CBM} = -3.166\ eV$ and $E^{Abs}_{VBM} = -4.579\ eV$ are obtained. The band alignments of various 2D materials compared with band offsets of SmN with respect to water's reduction and oxidation potentials are displayed in Fig. 10. The materials with straddle band offsets can be suitable for overall water splitting such as TiO_2 [62], ZnO [63], and BSe [64], otherwise they can only perform oxidation or reduction of water according to their VBM and CBM positions as shown in Fig. 10. One can find from

Fig. 10 that CBM of the SmN monolayer is much higher in potential than −4.39 eV and it is suitable for water reduction, but VBM cannot oxidize water molecules as it is higher than −5.62 eV similar to GaAs [25] and InP [65]. Hence, 2D SmN is suitable for the water reduction at neutral pH and can generate hydrogen by reducing the water molecules. To further unveil the micro-mechanism of hydrogen production by photocatalysis on the SmN monolayer, we simulated the interaction of two hydrogen adatoms as shown in Fig. 11. The hydrogen

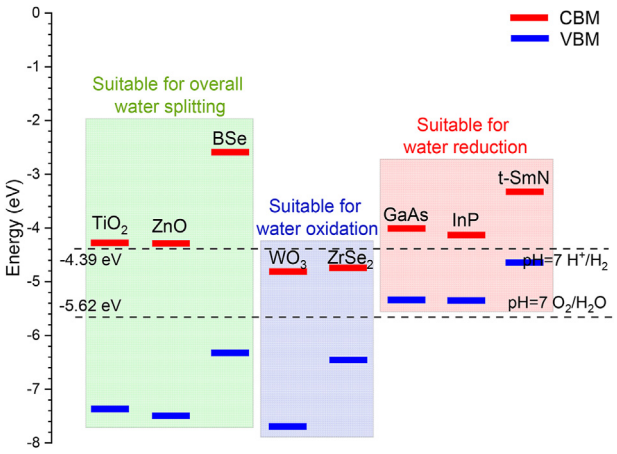

Fig. 10 – A comparison of band alignments of some 2D materials and SmN with respect to the water oxidation and reduction potentials for water splitting at 7 pH.

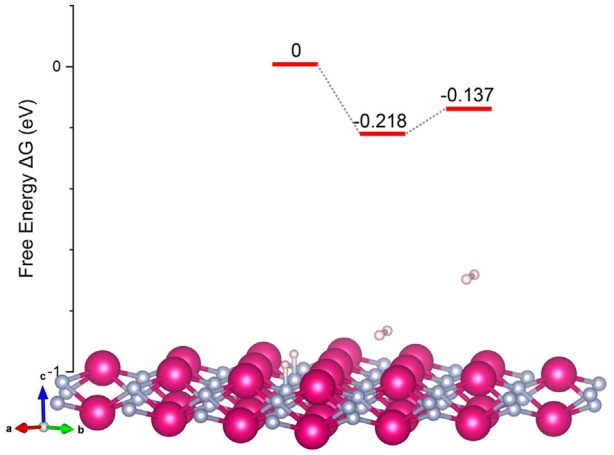

Fig. 11 – Pathway of the interaction between two hydrogen adatoms to form and release hydrogen molecule from the t-SmN monolayer.

atoms, produced by the water molecules' decomposition, are adsorbed on the adjacent nitrogen positions on the SmN monolayer [66]. The small endothermic reaction energy of 0.081 eV is required to remove the hydrogen molecule from SmN as displayed in Fig. 11 and it is easy for H_2 gas to be released. Hence, we can conclude that the SmN monolayer is an efficient photocatalyst for water splitting. On the other hand, this small endothermic reaction energy also implies that the SmN monolayer can be a potential material for hydrogen storage. Furthermore, small bandgap, optical absorption in visible region make and exothermic water decomposition make SmN monolayer an efficient photocatalyst over other 2D materials such as TiO_2, BSe, GaAs etc [52].

Conclusion

In summary, we studied the structural, electronic, optical, and photocatalytic properties of the t-SmN monolayer by performing first-principles calculations. The 2D SmN belongs to the P2_1/m space group and its lattice parameters are $a = 4.6671$ Å and $b = 4.0077$ Å. The absence of negative frequency modes in phonon band structure and low cohesive energy value of $-7.318\,eV$ exhibited its kinetic stability. Thermal and chemical stability of the SmN was proved by AIMD simulations. The 2D SmN was found a ferromagnetic semiconductor with direct bandgap of 1.41 eV by HSE06 calculations. Sm-4f electrons were responsible for spin polarization in the electronic structure. The hybridization of N-2p and Sm-5d states was found in VB and CB was mainly made of Sm-4f states. SmN also exhibited good optical absorption ability in the visible and ultraviolet region of solar spectrum. The calculated electronic and optical properties indicate that SmN monolayer is a robust photocatalytic material to convert solar energy into chemical energy. The band alignment was pointing the hydrogen evolution reaction only on the SmN monolayer. Finally, the study of water molecule dissociative absorption and hydrogen molecule formation on the SmN monolayer indicates that splitting of H_2O and formation of H_2 is energetically favourable on this monolayer. SmN monolayer can be considered as promising efficient photocatalyst for hydrogen formation by solar splitting water.

Ethical approval

Not applicable.

Funding

The authors sincerely appreciate funding from Researchers Supporting Project number (RSP2023R399), King Saud University, Riyadh, Saudi Arabia.

Availability of data and materials

Not applicable.

Declaration of Competing Interest

The authors declare that they have no known competing financial interests or personal relationships that could have appeared to influence the work reported in this paper.

REFERENCES

[1] Liu Z, He T, Jiang Q, Wang W, Tang J. A review of heteroatomic doped two-dimensional materials as electrocatalysts for hydrogen evolution reaction. Int J Hydrogen Energy 2022;47(69):29698–729.
[2] Majid A, et al. A density functional theory study of electronic properties of transition metals doped silicon carbide monolayer. Int J Quant Chem 2022;122(9):e26877.
[3] Wang C, Tang C, Fu L. An effective method to screen carbon (boron, nitrogen) based two-dimensional hydrogen storage materials. Int J Hydrogen Energy 2020;45(46):25054–64.

[4] Isa Khan M, et al. A DFT study on a borophene/boron nitride interface for its application as an electrode. Phys Chem Chem Phys 2020;22(6):3304–13.
[5] Liu W, et al. Two-dimensional ferromagnetic semiconductors of rare-earth monolayer GdX2 (X = Cl, Br, I) with large perpendicular magnetic anisotropy and high Curie temperature. Materials Today Physics 2021;21:100514.
[6] Lee Y, et al. Fabrication and imaging of monolayer phosphorene with preferred edge configurations via graphene-assisted layer-by-layer thinning. Nano Lett 2020;20(1):559–66.
[7] Yuan Z, Fan Y, Chen Y, Liu X, Liu B, Han S. Two-dimensional C@ TiO2/Ti3C2 composite with superior catalytic performance for NaAlH4. Int J Hydrogen Energy 2020;45(41):21666–75.
[8] Kośmider K, González JW, Fernández-Rossier J. Large spin splitting in the conduction band of transition metal dichalcogenide monolayers. Phys Rev B 2013;88(24):245436.
[9] Wang G, et al. Control of exciton valley coherence in transition metal dichalcogenide monolayers. Phys Rev Lett 2016;117(18):187401.
[10] Acun A, et al. Germanene: the germanium analogue of graphene. J Phys Condens Matter 2015;27(44):443002.
[11] Gonzalez JM, Oleynik II. Layer-dependent properties ofSnS2andSnSe2two-dimensional materials. Phys Rev B 2016;94(12):125443.
[12] Jiang X, et al. Recent progress on 2D magnets: fundamental mechanism, structural design and modification. Appl Phys Rev 2021;8(3):031305.
[13] Wijethunge D, et al. Tuning band alignment and optical properties of 2D van der Waals heterostructure via ferroelectric polarization switching. Frontiers of Physics 2020;15(6):63504 [${article.jieShuYe}].
[14] Majid A, et al. Layered silicon carbide: a novel anode material for lithium ion batteries. New J Chem 2021;45(40):19105–17.
[15] Yang Y, et al. FeS2-anchored transition metal single atoms for highly efficient overall water splitting: a DFT computational screening study. J Mater Chem 2021;9(4):2438–47.
[16] Pan H. Metal dichalcogenides monolayers: novel catalysts for electrochemical hydrogen production. Sci Rep 2014;4(1):5348.
[17] Wei Y, Huang H, Gao F, Jiang G. 2D transitional-metal nickel compounds monolayer: highly efficient multifunctional electrocatalysts for the HER, OER and ORR. Int J Hydrogen Energy 2023;48(11):4242–52.
[18] Liu G, et al. Unique physicochemical properties of two-dimensional light absorbers facilitating photocatalysis. Chem Soc Rev 2018;47(16):6410–44.
[19] Wu JM, Qi B. Low-temperature growth of monolayer rutile TiO2 nanorod films. J Am Ceram Soc 2007;90(2):657–60.
[20] Mahler B, et al. Colloidal synthesis of 1T-WS2 and 2H-WS2 nanosheets: applications for photocatalytic hydrogen evolution. J Am Chem Soc 2014;136(40):14121–7.
[21] Hong HK, et al. Atomic scale study on growth and heteroepitaxy of ZnO monolayer on graphene. Nano Lett 2017;17(1):120–7.
[22] Ying Y, et al. Theoretical investigation of monolayer RhTeCl semiconductors as photocatalysts for water splitting. J Phys Chem C 2019;124(1):639–46.
[23] Guo Z, et al. MXene: a promising photocatalyst for water splitting. J Mater Chem 2016;4(29):11446–52.
[24] Ying Y, et al. Theoretical investigation of monolayer RhTeCl semiconductors as photocatalysts for water splitting. J Phys Chem C 2020;124(1):639–46.
[25] Liu T, Bai L, Tian N, Liu J, Zhang Y, Huang H. Interfacial engineering in two-dimensional heterojunction photocatalysts. Int J Hydrogen Energy 2023;;48(33):12257–87.
[26] Leduc J, et al. Rare-Earth-containing materials for photoelectrochemical water splitting applications. In: Mi Z, Wang L, Jagadish C, editors. Semiconductors for photocatalysis. Elsevier; 2017. p. 185–219.
[27] Kresse G, Furthmuller J. Efficient iterative schemes for ab initio total-energy calculations using a plane-wave basis set. Phys Rev B Condens Matter 1996;54(16):11169–86.
[28] Perdew JP, Burke K, Ernzerhof M. Generalized gradient approximation made simple. Phys Rev Lett 1996;77(18):3865–8.
[29] Aynyas M, et al. Properties of samarium nitride: first principle calculations. AIP Conf Proc 2016;1728(1):020015.
[30] Som NN, et al. Magnetic behavior study of samarium nitride using density functional theory. J Magn Magn Mater 2018;448:186–91.
[31] Azmat MM, et al. First-principles study of antiferromagnetic superexchange interactions between TiAl-VN complexes in AlN. J Supercond Nov Magnetism 2022;35(3):889–98.
[32] Liao J, et al. Design of high-efficiency visible-light photocatalysts for water splitting: MoS2/AlN(GaN) heterostructures. J Phys Chem C 2014;118(31):17594–9.
[33] Sa B, et al. Strain engineering for phosphorene: the potential application as a photocatalyst. J Phys Chem C 2014;118(46):26560–8.
[34] Guo Z, et al. Band gap engineering in huge-gap semiconductor SrZrO3 for visible-light photocatalysis. Int J Hydrogen Energy 2014;39(5):2042–8.
[35] Yang X, et al. Two-dimensional aluminum phosphide semiconductor with tunable direct band gap for nanoelectric applications. RSC Adv 2020;10(42):25170–6.
[36] Martyna GJ, Klein ML, Tuckerman M. Nosé–Hoover chains: the canonical ensemble via continuous dynamics. J Chem Phys 1992;97(4):2635–43.
[37] Zhang X, et al. Tetragonal-structured anisotropic 2D metal nitride monolayers and their halides with versatile promises in energy storage and conversion. J Mater Chem 2017;5(6):2870–5.
[38] Xu B, et al. A two-dimensional tetragonal yttrium nitride monolayer: a ferroelastic semiconductor with switchable anisotropic properties. Nanoscale 2018;10(1):215–21.
[39] Thomsen C, Reich S, Ordejón P. Ab initiodetermination of the phonon deformation potentials of graphene. Phys Rev B 2002;65(7):073403.
[40] Yang LM, et al. Revealing unusual chemical bonding in planar hyper-coordinate Ni2Ge and quasi-planar Ni2Si two-dimensional crystals. Phys Chem Chem Phys 2015;17(39):26043–8.
[41] Topsakal M, et al. First-principles study of zinc oxide honeycomb structures. Phys Rev B 2009;80(23):235119.
[42] Beshkova M, Yakimova R. Properties and potential applications of two-dimensional AlN. Vacuum 2020;176:109231.
[43] Xu B, et al. A two-dimensional tetragonal yttrium nitride monolayer: a ferroelastic semiconductor with switchable anisotropic properties. Nanoscale 2017;10(1):215–21.
[44] Cahangirov S, et al. Two- and one-dimensional honeycomb structures of silicon and germanium. Phys Rev Lett 2009;102(23):236804.
[45] Molina-Sánchez A, Wirtz L. Phonons in single-layer and few-layer MoS$_{2}$ and WS$_{2}$. Phys Rev B 2011;84(15):155413.
[46] Huang LF, Gong PL, Zeng Z. Correlation between structure, phonon spectra, thermal expansion, and thermomechanics of single-layerMoS2. Phys Rev B 2014;90(4):045409.
[47] Li Z, Shi D, Yang J, Luo W, Wan C, Pan W. Contribution of optical phonons to lattice thermal conductivity in complex structural thermal insulation materials. J Eur Ceram Soc 2021;41(15):7981–7.

[48] Yang J, Li LL, Li JR, Yang JX, Zhang F, Chen G, Wu SW. Synthesis and biological evaluation of water-soluble derivatives of chiral gossypol as HIV fusion inhibitors targeting gp41. Bioorg Med Chem Lett 2018;28(1):49–52.
[49] Toberer ES, Zevalkink A, Snyder GJ. Phonon engineering through crystal chemistry. J Mater Chem 2011;21(40):15843–52.
[50] (a). Jia M, Yang CL, Wang MS, Ma XG. Excellent thermoelectric performances of the SiSe2 monolayer and layered bulk. Appl Surf Sci 2022;575:151799.

(b). Jia M, Yang CL, Wang MS, Ma XG. High dimensionless figure of merit of the ZrI2 monolayer identified based on intrinsic carrier concentration and bipolar effect. Appl Phys Lett 2022;121(12):123903.
[51] Granville S, et al. Vibrational properties of rare-earth nitrides: Raman spectra and theory. Phys Rev B 2009;79(5):054301.
[52] Li SS, Ji WX, Hu SJ, Zhang CW, Yan SS. Effect of amidogen functionalization on quantum spin Hall effect in Bi/Sb (111) films. ACS Appl Mater Interfaces 2017;9(47):41443–53.
[53] Sun H, Li SS, Ji WX, Zhang CW. Valley-dependent topological phase transition and quantum anomalous valley Hall effect in single-layer RuClBr. Phys Rev B 2022;105(19):195112.
[54] Li KN, Yang CL, Wang MS, Ma XG, Wang LZ. Extraction of H2 from H2O molecule using a small Al6Si cluster. Int J Hydrogen Energy 2016;41(40):17858–63.
[55] Li KN, Yang CL, Han YX, Wang MS, Ma XG, Wang LZ. Generating H2 from a H2O molecule by catalysis using a small Al6Cu cluster. Energy 2016;106:131–6.
[56] Ma X, Shi Y, Liu J, Li X, Cui X, Tan S, Wang B. Hydrogen-bond network promotes water splitting on the TiO2 surface. J Am Chem Soc 2022;144(30):13565–73.
[57] Wang F, Yang CL, Wang MS, Ma X. Photocatalytic hydrogen evolution reaction with high solar-to-hydrogen efficiency driven by the Sb2S3 monolayer and RuI2/Sb2S3 heterostructure with solar light. J Power Sources 2022;532:231352.
[58] Sun R, et al. High solar-to-hydrogen efficiency photocatalytic hydrogen evolution reaction with the HfSe2/InSe heterostructure. J Power Sources 2022;547:232008.
[59] Zhang CF, Yang CL, Wang MS, Ma XG. Z-Scheme photocatalytic solar-energy-to-hydrogen conversion driven by the HfS 2/SiSe heterostructure. J Mater Chem C 2022;10(14):5474–81.
[60] Yin QK, Yang CL, Wang MS, Ma XG. Two-dimensional heterostructures of AuSe/SnS for the photocatalytic hydrogen evolution reaction with a Z-scheme. J Mater Chem C 2021;9(36):12231–8.
[61] Zhao Z, Li Z, Zou Z. A theoretical study of water adsorption and decomposition on the low-index stoichiometric anatase TiO2 surfaces. J Phys Chem C 2012;116(13):7430–41.
[62] Yang X, Singh D, Ahuja R. Recent advancements and future prospects in ultrathin 2D semiconductor-based photocatalysts for water splitting. Catalysts 2020;10(10):1111.
[63] Do TN, et al. Type-I band alignment of BX-ZnO (X = As, P) van der Waals heterostructures as high-efficiency water splitting photocatalysts: a first-principles study. RSC Adv 2020;10(72):44545–50.
[64] Ren K, Yu J, Tang W. Two-dimensional ZnO/BSe van der waals heterostructure used as a promising photocatalyst for water splitting: a DFT study. J Alloys Compd 2020;812:152049.
[65] Chen L, Zhou X, Yu J. First-principles study on the electronic and optical properties of the ZnTe/InP heterojunction. J Comput Electron 2019;18(3):749–57.
[66] Qureshi WA, Haider SNUZ, Naveed A, Ali A, Liu Q, Yang J. Recent progress in the synthesis, characterization and photocatalytic application of energy conversion over single metal atoms decorated graphitic carbon nitride. Int J Hydrogen Energy 2023. https://doi.org/10.1016/j.ijhydene.2022.11.181.